Exchange between interstitial oxygen molecules and network oxygen atoms in amorphous SiO_2 studied by ^{18}O isotope labeling and infrared photoluminescence spectroscopy

Koichi Kajihara,[1,*] Taisuke Miura,[2] Hayato Kamioka,[3] Masahiro Hirano,[4,5] Linards Skuja,[6] and Hideo Hosono[5,7]

[1]*Department of Applied Chemistry, Graduate School of Urban Environmental Sciences,Tokyo Metropolitan University, 1-1 Minami-Osawa, Hachioji 192-0397, Japan*

[2]*Research and Development Division, OMRON Laserfront Inc., 1120 Shimokuzawa, Sagamihara 229-1198, Japan*

[3]*Graduate School of Pure and Applied Sciences, University of Tsukuba,1-1-1 Tennodai, Tsukuba 305-8571, Japan*

[4]*Japan Science and Technology Agency, Nibancho Chiyoda ku, Tokyo 102-0084, Japan*

[5]*Frontier Research Center, Tokyo Institute of Technology, 4259 Nagatsuta, Midori-ku, Yokohama 226-8503, Japan*

[6]*Institute of Solid State Physics, University of Latvia, Kengaraga iela 8, LV-1063 Riga, Latvia*

[7]*Materials and Structures Laboratory, Tokyo Institute of Technology, 4259 Nagatsuta, Midori-ku, Yokohama 226-8503, Japan*

(Received 29 October 2010; revised manuscript received 4 January 2011; published 25 February 2011)

Amorphous SiO_2 (a-SiO_2) thermally annealed in an oxygen atmosphere incorporates oxygen molecules (O_2) in interstitial voids. When the thermal annealing is performed in $^{18}O_2$ gas, interstitial $^{18}O_2$ as well as interstitial $^{16}O^{18}O$ and $^{16}O_2$ are formed due to the oxygen exchange with the a-SiO_2 network. The $a^1\Delta_g(v = 0) \rightarrow X^3\Sigma_g^-(v = 1)$ infrared photoluminescence band of interstitial O_2 was utilized to quantitatively analyze the oxygen exchange, taking into account the influences of common network modifiers in synthetic a-SiO_2 (SiOH, SiF, and SiCl groups). The presence of network modifiers does not significantly change the average rate of ^{18}O transfer from interstitial O_2 to the a-SiO_2 network and its activation energy, suggesting that the network modifiers themselves do not serve as preferential oxygen exchange sites. When the concentration of SiOH groups is low, the oxygen exchange rate is distributed, indicating that only a small part of the network oxygen atoms participates in the oxygen exchange. However, the distribution of the oxygen exchange rate is distinctly narrow in the sample with high SiOH concentration. It is attributed to the redistribution of the network ^{18}O atoms and the modification of the a-SiO_2 network topology caused by reactions with mobile interstitial water molecules, which are transiently formed by dehydroxylation of paired SiOH groups. The activation energy for the average oxygen exchange rate is larger than that of the permeation of interstitial O_2 in a-SiO_2. Furthermore, the average exchange-free diffusion length of interstitial O_2 below 900 °C ($\gtrsim 1\ \mu$m) is far larger than the scale of the interstitial voids in a-SiO_2 ($\lesssim 1$ nm). These observations confirm that the oxygen exchange is not necessarily involved in the permeation of interstitial O_2.

DOI: 10.1103/PhysRevB.83.064202 PACS number(s): 61.72.jj, 65.60.+a, 66.30.hh, 78.55.Qr

I. INTRODUCTION

The growth kinetics and mechanisms of amorphous SiO_2 (a-SiO_2) on silicon by thermal oxidation have been extensively studied to improve the electronic properties of a-SiO_2 films, in particular, ultrathin gate-dielectric layers[1] required to further scale down the silicon-based microelectronic circuits. A key step in growing a-SiO_2 is oxygen transport to the silicon-oxide interface, which is governed by the permeation of interstitial oxygen molecules (O_2) dissolved in interstices of an a-SiO_2 network.[2,3] It is generally considered that interstitial O_2 permeates through the interstices without strongly interacting with the a-SiO_2 network.[4–7] On the other hand, observations by secondary ion mass spectroscopy (SIMS)[8–13] and nuclear reaction analysis (NRA)[13–16] of $^{18}O_2$-treated a-SiO_2 on silicon have confirmed the incorporation of ^{18}O in the a-SiO_2 network, indicating that interstitial O_2 does replace network oxygen atoms in a-SiO_2. However, both SIMS and NRA are insensitive to the oxygen bonding states and are therefore incapable of detecting interstitial O_2 on the background of network oxygens that is several orders-of-magnitude stronger. In addition, incorporation of ^{18}O from ^{18}O-labeled water molecules, inadvertently generated by reactions between ambient $^{18}O_2$ gas and trace water in it, complicates the analysis of SIMS and NRA data. Indeed, ^{18}O profiles observed by SIMS and NRA near the sample surface are most likely formed by reactions involving interstitial water molecules, rather than by the simple incorporation of ^{18}O from interstitial O_2 and self-diffusion of ^{18}O-labeled network oxygen atoms.[6,17] Thus, a reliable study of oxygen exchange between interstitial O_2 and the network oxygen atoms in a-SiO_2 has remained a formidable task.

We developed a photoluminescence (PL) technique to study diffusion and reactions of interstitial O_2 in a-SiO_2.[18] Figure 1 shows a PL spectrum of interstitial O_2 excited via the transition from the ground state $X^3\Sigma_g^-(v = 0)$ to the second singlet excited state $b^1\Sigma_g^+(v = 0)$ at 765 nm.[19] This excitation induces two PL bands associated with transitions from the first excited singlet state $a^1\Delta_g(v = 0)$: an intense PL band at $\sim$7855 cm^{-1} attributed to the transition to the $X^3\Sigma_g^-(v = 0)$ state (pure electronic band, PEB), and a much weaker PL band at $\sim$6308 cm^{-1} due to the transition to the first vibronic level of the X state $X^3\Sigma_g^-(v = 1)$ (vibrational sideband, VSB).[19] The PEB is negligibly shifted by oxygen isotopic substitution, whereas the VSB is coupled to the O–O stretching mode of O_2 and exhibits a large isotope shift. Thus, isotopic composition of interstitial O_2 can be determined from the shape of the VSB spectrum. In the preceding paper,[20] we show that this PL technique provides direct information on the oxygen exchange between interstitial O_2 and the network oxygen atoms in a-SiO_2. The purpose of the present paper is to examine contributions of common network modifiers

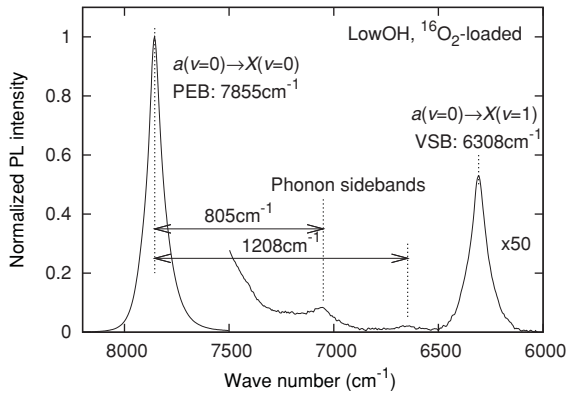

FIG. 1. A PL spectrum of an O_2-rich LowOH sample prepared by thermal annealing in $^{16}O_2$. Vibrational sideband (VSB) at ~6300 cm^{-1} is sensitive to the isotopic composition of interstitial O_2.

(SiOH, SiF, and SiCl groups) in synthetic a-SiO_2 to the oxygen exchange. Based on the results, the influence of trace water impurities on the oxygen exchange will be discussed.

II. EXPERIMENTAL PROCEDURE

A. Sample preparation and measurements

Three types of synthetic a-SiO_2 samples were used: "LowOH" (SiOH, $\sim 2 \times 10^{18}$ cm^{-3}), "HighOH" (SiOH, $\sim 1 \times 10^{20}$ cm^{-3}; SiCl, $\sim 5 \times 10^{18}$ cm^{-3}), and "F-doped" (SiOH, ~ 1–2×10^{18} cm^{-3}; SiF, $\sim 1.4 \times 10^{19}$ cm^{-3}). They were cut into specimens in the form of $10 \times 6.5 \times 0.4$–0.5 mm^3 and the two largest faces were polished to an optical finish. These specimens were sealed in an SiOH-free silica tube (SiOH $\lesssim 10^{17}$ cm^{-3}, ~10 cm long, ~12 mm inner diameter, and ~1.2 mm thick) with $^{18}O_2$ (^{18}O isotopic purity $\gtrsim$99%) or $^{16}O_2$ gas of 0.9 atm at room temperature. The sealed silica tubes, each containing eight equivalent specimens, were thermally annealed between 500 and 900 °C to incorporate ^{18}O-labeled interstitial O_2 into the specimens. The isotopic composition of O_2 gas in the silica tube was monitored before and after the thermal annealing by a self-made Raman spectrometer.[21] After the thermal annealing, the specimens were taken out from the tube and the PL spectra were measured by a Fourier-transform Raman spectrometer (Model 960, Nicolet) with a spectral resolution of 8 cm^{-1} under excitation at 765 nm with an AlGaAs laser diode (spectral linewidth ~2 nm, ~1.5 W at sample position). The specimens were irradiated normal to the polished face and the backscattered PL emission was recorded. The VSB spectra, which have a very weak intensity (Fig. 1), were measured using stacks of the eight equivalent specimens. On the other hand, the relative PEB intensity was measured using a single specimen to minimize uncertainties due to surface reflection.

The thickness average of the total concentration of interstitial O_2, C_a^T, in the O_2-loaded specimens was evaluated by comparing the relative PEB intensity with that of a reference sample of a known interstitial $^{16}O_2$ concentration.[18,22] However, a correction due to changing fractions of interstitial $^{16}O_2$, $^{16}O^{18}O$, and $^{18}O_2$ (f_{66}, f_{68}, and f_{88}, respectively, where $f_{66} + f_{68} + f_{88} = 1$) is necessary, since PL decay constant τ increases in the order of interstitial $^{16}O_2$, $^{16}O^{18}O$, and $^{18}O_2$ ($\tau_{66} < \tau_{68} < \tau_{88}$), and τ is proportional to the PL quantum yield of the PEB.[23] Thus, the variation of the "effective" PL quantum yield with the fractions of ^{18}O-labeled interstitial O_2 was accounted for by multiplying the observed PEB intensity by a factor $f_{66}\tau_{66}/(f_{66}\tau_{66} + f_{68}\tau_{68} + f_{88}\tau_{88})$. f_{66}, f_{68}, and f_{88} were evaluated by simple peak decomposition of the VSB spectrum using three pseudo-Voigt peak functions with peak parameters that were predetermined, as described in Refs. 20 and 23. The PL decay curves of the PEB were measured using stacks of the eight specimens. The details of the measurement and data analysis are reported in Refs. 23 and 24. Briefly, τ values were evaluated by fitting the observed normalized PL decay curve to a linear combination of three stretched exponential functions,

$$I_{\mathrm{norm}}(t) = \sum_{i=66,68,88} f_i \exp[-(t/\tau_i)^{\beta}]. \tag{1}$$

The stretched exponent β and τ_{66} were fixed to the values determined for an ^{18}O-free sample, and τ_{68} and τ_{88} were treated as variables. The most probable τ_{68} and τ_{88} values were calculated by taking their averages for all samples using f_{68} and f_{88} of each sample as the weighting values.

B. Data analysis

We assumed that network oxygen atoms exchange only with interstitial O_2, that in each exchange event only one of two oxygen atoms in an O_2 molecule is replaced, and that the exchange is characterized by a second-order rate constant k. Self-diffusion of network oxygen atoms[4,25] was neglected because it is very slow. Other reactions to redistribute network oxygen, e.g., reactions caused by residual water,[6,17] were not considered explicitly. Thus, exchange involving ^{18}O may be described as[26,27]

$$^{18}O^{18}O + \equiv Si-{}^{16}O-Si\equiv \rightleftarrows {}^{16}O^{18}O + \equiv Si-{}^{18}O-Si\equiv, \tag{2}$$

$$^{16}O^{18}O + \equiv Si-{}^{16}O-Si\equiv \rightleftarrows {}^{16}O^{16}O + \equiv Si-{}^{18}O-Si\equiv. \tag{3}$$

The rate constants for the Eq. (2) forward and Eq. (3) backward reactions are k. However, the rate constants for the Eq. (2) backward and Eq. (3) forward reactions should apparently be $k/2$ because the exchange between the same oxygen isotopes is not detectable. It is most likely that k is a function of the configuration of the network oxygen atom, such as the local network topology around it and the Si–O–Si angle. Thus, k may be different from site to site in a-SiO_2 due to the structural disorder. The corresponding k distribution was considered by simply assuming a Gaussian distribution of activation energy for k. This is equivalent to the condition that the fraction of the network oxygen atoms associated with k follows a Gaussian distribution function g against $\log k$ as follows:

$$g(\log k) = \frac{1}{c\pi^{1/2}} \exp\left[-\left(\frac{\log k - \log k_{\mathrm{peak}}}{c}\right)^2\right], \quad \text{where} \quad c = \frac{w}{2(\ln 2)^{1/2}}, \tag{4}$$

and where w denotes the full width at half maximum (FWHM) of the distribution in a decimal logarithmic scale.[28] The distribution was approximated by a set of $2I+1$ discrete components separated by a constant step in $\log k$ space, and defined by

$$\log k_i - \log k_{\text{peak}} = \frac{iRc}{I}, \tag{5}$$

where i and I are integers satisfying $|i| \leqq I$, and R is the integration range of the distribution. We employed $I = 15$ and $R = 4$ in this study, and confirmed that further increase in these values did not change the results. The concentration of the network oxygen atom in component i, N_i^{T}, is given by

$$N_i^{\text{T}} = \frac{g(\log k_i)}{\sum_i g(\log k_i)} N^{\text{T}}, \tag{6}$$

where $N^{\text{T}} = \sum_i N_i^{\text{T}}$ is the total concentration of the network oxygen atom (4.41×10^{22} cm^{-3}).[17] It was assumed that w is inversely proportional to the absolute temperature T, indicating that the distribution of the activation energy for k is independent of T.[28] However, explicit correlation between T and $k_{\text{peak}} = k_{i=0}$, such as the Arrhenius-type dependence of k_{peak} on T, was not postulated.

The concentration profiles of interstitial $^{16}O_2$, $^{16}O^{18}O$, and $^{18}O_2$ [$C(x,t)$, $C^*(x,t)$, and $C^{**}(x,t)$, respectively] were calculated by solving simultaneous rate equations for one-dimensional diffusion and exchange reactions in a plane sheet (thickness L) occupying the region $-L/2 \leqq x \leqq L/2$,

$$\frac{\partial C}{\partial t} = D\frac{\partial^2 C}{\partial x^2} + \sum_i k_i \left(\frac{1}{2} C^* N_i - C N_i^* \right), \tag{7}$$

$$\frac{\partial C^*}{\partial t} = D\frac{\partial^2 C^*}{\partial x^2} + \sum_i k_i \left(-\frac{1}{2} C^* N_i + C^{**} N_i + C N_i^* - \frac{1}{2} C^* N_i^* \right), \tag{8}$$

$$\frac{\partial C^{**}}{\partial t} = D\frac{\partial^2 C^{**}}{\partial x^2} + \sum_i k_i \left(- C^{**} N_i + \frac{1}{2} C^* N_i^* \right), \tag{9}$$

where D denotes the diffusion coefficient of interstitial O_2 in a-SiO_2. The combination of Eqs. (7)–(9) yields the diffusion equation for the total concentration of interstitial O_2, $C^{\text{T}}(x,t) \equiv C + C^* + C^{**}$,

$$\frac{\partial C^{\text{T}}}{\partial t} = D\frac{\partial^2 C^{\text{T}}}{\partial x^2}. \tag{10}$$

The rate equation for the network ^{16}O and ^{18}O atoms belonging to the component i [$N_i(x,t)$ and $N_i^*(x,t) = N_i^{\text{T}} - N_i(x,t)$, respectively] is expressed by

$$\begin{aligned} \frac{\partial N_i^*}{\partial t} = -\frac{\partial N_i}{\partial t} &= k_i \left(\frac{1}{2} C^* N_i + C^{**} N_i - C N_i^* - \frac{1}{2} C^* N_i^* \right) \\ &= k_i \left[C^{\text{T}} N_i - \frac{1}{2}(2C + C^*) N_i^{\text{T}} \right] \\ &= -k_i \left[C^{\text{T}} N_i^* - \frac{1}{2}(2C^{**} + C^*) N_i^{\text{T}} \right]. \end{aligned} \tag{11}$$

Substitution of Eq. (11) into Eqs. (7)–(9) yields rate equations for the concentrations of ^{16}O or ^{18}O atoms in interstitial O_2 and the a-SiO_2 network,

$$\frac{\partial (2C + C^*)}{\partial t} = D\frac{\partial^2 (2C + C^*)}{\partial x^2} + \sum_i k_i \left[C^{\text{T}} N_i - \frac{1}{2}(2C + C^*) N_i^{\text{T}} \right], \tag{12}$$

$$\frac{\partial (2C^{**} + C^*)}{\partial t} = D\frac{\partial^2 (2C^{**} + C^*)}{\partial x^2} + \sum_i k_i \left[C^{\text{T}} N_i^* - \frac{1}{2}(2C^{**} + C^*) N_i^{\text{T}} \right] \tag{13}$$

These equations are rewritten to k_i-free forms,

$$\frac{\partial (2C + C^*)}{\partial t} = D\frac{\partial^2 (2C + C^*)}{\partial x^2} - \frac{\partial N}{\partial t}, \tag{14}$$

$$\frac{\partial (2C^{**} + C^*)}{\partial t} = D\frac{\partial^2 (2C^{**} + C^*)}{\partial x^2} - \frac{\partial N^*}{\partial t}, \tag{15}$$

where $N(x,t) \equiv \sum_i N_i(x,t)$ and $N^*(x,t) \equiv \sum_i N_i^*(x,t) = N^{\text{T}} - N(x,t)$ denote the total concentrations of the network ^{16}O and ^{18}O atoms, respectively.

The average oxygen exchange rate may be given by the weighted average of k_i as

$$k_{\text{a}} = \sum_i k_i \frac{N_i^{\text{T}}}{N^{\text{T}}}. \tag{16}$$

However, k_{a} cannot be easily related to experimental observations. As defined by Eq. (16), it is independent of x and t. In contrast, the observable, "effective" exchange rate k_{eff} must depend on x and t, since the subset of sites characterized by faster exchange rates k_i and located at some arbitrary position x will approach the equilibrium condition $N_i^*(x,t)/N_i^{\text{T}} = [C^*(x,t)/2 + C^{**}(x,t)]/C^{\text{T}}(x,t)$ earlier than sites having smaller k_i values, resulting in a gradual decrease in the effective exchange rate. It may be defined by Eq. (17), which can be regarded as the sum of Eq. (11) for all i components,

$$\begin{aligned} \frac{\partial N^*}{\partial t} = -\frac{\partial N}{\partial t} &= k_{\text{eff}} \left(\frac{1}{2} C^* N + C^{**} N - C N^* - \frac{1}{2} C^* N^* \right) \\ &= k_{\text{eff}} \left[\frac{1}{2}(2C^{**} + C^*) N^{\text{T}} - C^{\text{T}} N^* \right]. \end{aligned} \tag{17}$$

At $t = 0$, $k_{\text{eff}}(x,t)$ is equal to k_{a} at all x values because $C = C^* = 0$, $N^* = 0$, and $N = N^{\text{T}}$ in Eq. (17). The thickness average of k_{eff}, $k_{\text{eff,a}}(t)$, may be defined using a functional $h(z)$,

$$h(z) = \frac{1}{L}\int_{-L/2}^{L/2} z(x,t)dx = z_{\text{a}}(t), \tag{18}$$

and Eq. (17) as

$$h\left(\frac{\partial N^*}{\partial t}\right) = k_{\text{eff,a}} h\left[\frac{1}{2}(2C^{**} + C^*) N^{\text{T}} - C^{\text{T}} N^* \right], \tag{19}$$

$$\frac{\partial N_{\text{a}}^*}{\partial t} = k_{\text{eff,a}} \left[\frac{1}{2}(2C_{\text{a}}^{**} + C_{\text{a}}^*) N^{\text{T}} - h(C^{\text{T}} N^*) \right], \tag{20}$$

where the subscripts a for C and N denote their thickness averages. The difference between $k_{\text{eff,a}}(t)$ and k_{a} depends on

the degree of the distribution in k; $k_{\mathrm{eff,a}}$ is a constant equal to k_{a} when k is not distributed, whereas $k_{\mathrm{eff,a}}$ decreases with time when k is distributed.

The rate equations (7)–(9) were numerically solved[29] using the Crank-Nicolson finite-difference method provided that the sample initially contains neither interstitial O_2 nor network ^{18}O atoms, i.e., $C^{\mathrm{T}}(|x| < L/2, t = 0) = 0$ and $N^*(|x| \leqq L/2, t = 0) = 0$. It was also postulated that the sample surfaces are always saturated at C_0^{T} with interstitial $^{18}O_2$, $C^{\mathrm{T}}(x = \pm L/2, t) = C^{**}(x = \pm L/2, t) = C_0^{\mathrm{T}}$, because the dissolution of O_2 in a-SiO_2 is much faster than the following O_2 diffusion,[22,30] and the Raman analysis confirmed that the fraction of ^{18}O atoms in O_2 gas sealed in the silica tube was always close to 1 ($\gtrsim$0.97) even after the thermal O_2 loadings. From the solutions C, C^*, and C^{**}, the respective isotopic fractions were calculated using Eq. (18) as $f_{66} = C_{\mathrm{a}}/C_{\mathrm{a}}^{\mathrm{T}}$, $f_{68} = C_{\mathrm{a}}^*/C_{\mathrm{a}}^{\mathrm{T}}$, and $f_{88} = C_{\mathrm{a}}^{**}/C_{\mathrm{a}}^{\mathrm{T}}$. Using f_{66}, f_{68}, and f_{88} derived in this way, the VSB spectra were synthesized and then least-squares fitted to the observed spectra by treating k_{peak} at each temperature and w as variables. Each simulated spectrum consisted of three pseudo-Voigt functions with peak parameters that were predetermined.[20,23] All the spectra recorded for the same type of samples were fitted simultaneously. This direct spectral fitting of the VSB reduced uncertainties in determining f_{66}, f_{68}, and f_{88} compared with the simple peak decomposition.

III. RESULTS

A. Concentration change of interstitial O_2 by thermal oxygen loading

Table I lists PL decay constants of the PEB. The observed τ_{66} and β values agreed well with those reported previously.[24] The ratios τ_{68}/τ_{66} and τ_{88}/τ_{66} were almost independent of the sample type.

Figure 2 shows the variation of $C_{\mathrm{a}}^{\mathrm{T}}$ with time and temperature in the LowOH, HighOH, and F-doped samples. In each plot, $C_{\mathrm{a}}^{\mathrm{T}}$ increased linearly with $t^{1/2}L^{-1}$. The slope of the plot is equal to $4C_0^{\mathrm{T}}(D/\pi)^{1/2}$. (Refs. 22, 31) However, D and C_0^{T}, which are necessary for the numerical simulation, cannot be determined uniquely only from the slope. To evaluate D and C_0^{T} independently at each temperature, the observed data were compared with the theoretical concentration change given by solving Eq. (10),[22,31,32]

$$\frac{C_{\mathrm{a}}^{\mathrm{T}}(t)}{C_0^{\mathrm{T}}} = 1 - \frac{8}{\pi^2}\sum_{n=1}^{\infty}\frac{\exp[-D(2n-1)^2\pi^2 t/L^2]}{(2n-1)^2}. \qquad (21)$$

TABLE I. PL decay constants (in seconds) of interstitial $^{16}O_2$, $^{16}O^{18}O$, and $^{18}O_2$ (τ_{66}, τ_{68}, and τ_{68}, respectively) and the stretched exponent β evaluated using PEB PL and Eq. (1).

Type	τ_{66}[a]	τ_{68}[b]	τ_{88}[b]	β	τ_{68}/τ_{66}	τ_{88}/τ_{66}
LowOH	0.84	1.47	2.08	0.94	1.7	2.5
HighOH	0.69	1.17	1.64	0.89	1.7	2.4
F-doped	0.84	1.54	2.09	0.94	1.8	2.5

[a]Uncertainty: ±0.02 s
[b]Uncertainty: ±0.1 s

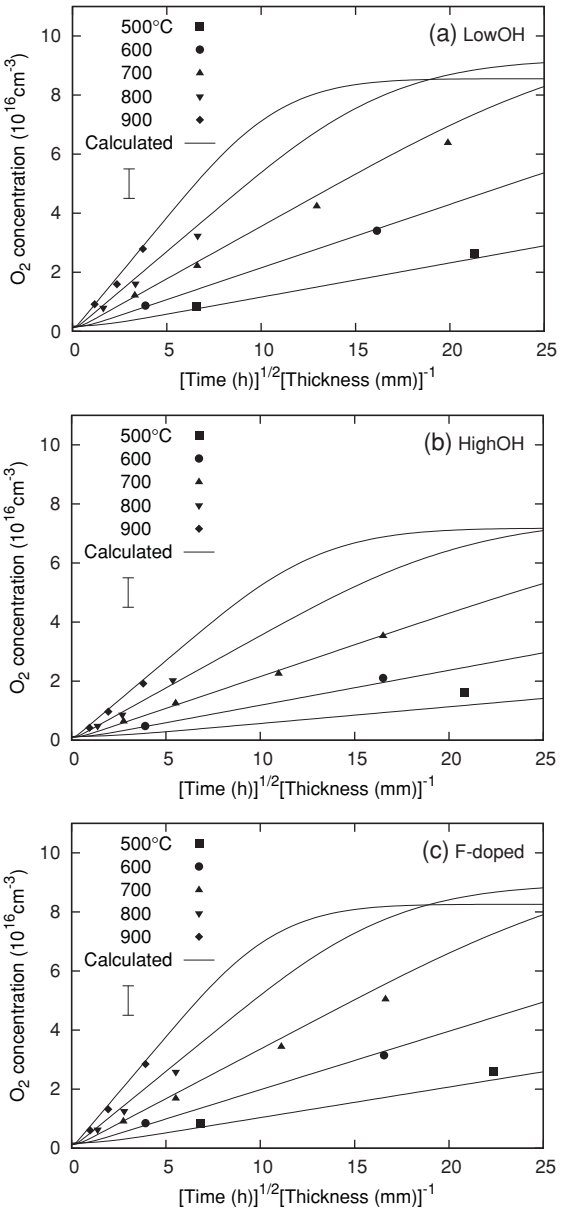

FIG. 2. Concentration of interstitial O_2 in the (a) LowOH, (b) HighOH, and (c) F-doped samples treated in $^{18}O_2$ between 500 and 900 °C. Filled symbols denote values determined from the PEB intensity. Solid lines are calculated by Eq. (21) using D and C_0^{T} derived from the Arrhenius-type relations of the diffusion coefficient and solubility defined by parameters listed in Table II. The error bar represents the experimental uncertainty.

D and the solubility S were derived from Arrhenius-type expressions. Their parameters were determined by separate experiments performed above 800 °C (Refs. 18, 22, 33) and are listed in Table II. C_0^{T} was calculated from S assuming that O_2 pressure inside the silica tube is roughly proportional to T of O_2 loading as $C_0^{\mathrm{T}} = Sp_{\mathrm{RT}}T/T_{\mathrm{RT}}$, where p_{RT} is the pressure of O_2 (0.9 atm) sealed in the silica tube at room temperature ($T_{\mathrm{RT}} = 298$ K). As shown in Fig. 2, the experimental and calculated data agree well. Thus, the simulation was performed using D and S derived from the Arrhenius parameters listed in Table II.

TABLE II. Arrhenius parameters to calculate the diffusion coefficient $D = D_0 \exp(-\Delta E_a/kT)$ and solubility $S = S_0 \exp(-\Delta H/kT)$ of interstitial O_2 in a-SiO_2.

Type	D_0(cm^{2}s^{-1})	ΔE_a(eV)	S_0(cm^{-3} atm^{-1})	ΔH(eV)
LowOH[d]	4.5×10^{-5}[a]	0.93[a]	4.2×10^{15}[c,e]	−0.18[c]
HighOH[d]	6.7×10^{-5}[a]	1.01[a]	4.8×10^{15}[c,e]	−0.15[c]
F-doped[f]	7.2×10^{-4}[b]	0.98[b]	3.9×10^{15}[c]	−0.18[c]

[a]Derived from data measured at 800, 900, 1000, 1100, and 1200 °C.
[b]Derived from data measured at 800, 900, 1000, and 1100 °C.
[c]Derived from data measured at 800, 900, and 1000 °C.
[d]Reference 22.
[e]Reference 18.
[f]Reference 33.

B. Variation of the isotopic composition of interstitial O_2 evaluated from the shape of the VSB spectra

Figure 3 shows the VSB spectra of LowOH, HighOH, and F-doped samples thermally annealed in $^{16}O_2$ or $^{18}O_2$ at 700 °C. The VSB of the $^{16}O_2$-treated sample was located at ∼6308 cm^{-1} and was simulated well with a pseudo-Voigt function.[20] In $^{18}O_2$-treated samples, on the contrary, two additional bands attributed to interstitial $^{16}O^{18}O$ and $^{18}O_2$ appeared at ∼6352 and ∼6397 cm^{-1}, respectively.[20] In all the samples, the fraction of ^{16}O atoms in interstitial O_2 ($1 - f^* \equiv f_{66} + f_{68}/2$) evaluated from the intensity ratio of VSBs increased with an increase in the annealing time because of the release of ^{16}O from the a-Si$^{16}O_2$ network. However, intensity changes of $^{16}O_2$ and $^{18}O_2$ bands between 2 and 72 h were obviously larger in the HighOH sample than in the LowOH and F-doped samples. The observed VSB spectra were fitted well with simulated spectra in all samples.

Figure 4 summarizes the time variations of f_{66} and f_{88} in the LowOH, HighOH, and F-doped samples. Lines denote simulated curves derived by the direct spectral fitting of the VSB (Sec. II B), and filled symbols indicate f_{66} and f_{88} evaluated by a simple VSB peak decomposition under the restriction condition $f_{66} + f_{68} + f_{88} = 1$. Figure 4 also shows that time dependences of f_{66} and f_{88} in the HighOH sample were different from those in the other two samples. In the HighOH sample, f_{66} and f_{88} showed sigmoidal dependences on $t^{1/2}$. On the other hand, the variations of the slopes of f_{66} and f_{88} curves with $t^{1/2}$ in the LowOH and F-doped samples were rather monotonic.

C. Temperature dependence of the rate of oxygen exchange between interstitial O_2 and the a-SiO_2 network

Figure 5 shows Arrhenius plots of $k_{eff,a}$ defined in Eq. (20) and calculated by simulating the data shown in Figs. 3 and 4. As described in Sec. II B, $k_{eff,a}$ represents the effective rate of uptake of ^{18}O from interstitial O_2 into the a-SiO_2 network; it is a constant when k is not distributed, whereas it decreases with time when k is distributed. To examine the effect of distribution in k on $k_{eff,a}$, $k_{eff,a}$ was calculated at $t = 0$ and at the moment when $C_a^T(t)/C_0^T = 0.5$, i.e., $t = 0.25t_c$, where $t_c = \pi(L/4)^2/D$.

$k_{eff,a}$ of the HighOH sample changed negligibly with t. In contrast, $k_{eff,a}$ of the LowOH and F-doped samples were larger than that of the HighOH sample at $t/t_c = 0$, but became smaller at $t/t_c = 0.25$. Despite these differences, the time average of $k_{eff,a}$ was comparable among these three samples, indicating that their overall rate of incorporation of ^{18}O into a-SiO_2 was similar. Furthermore, $\log k_{eff,a}$ changed almost linearly with T^{-1} in all samples, making it possible to evaluate the activation energy ΔE_a and the preexponential factor k_0, as summarized in Table III. ΔE_a was ∼2 eV, irrespective of the sample type and t/t_c.

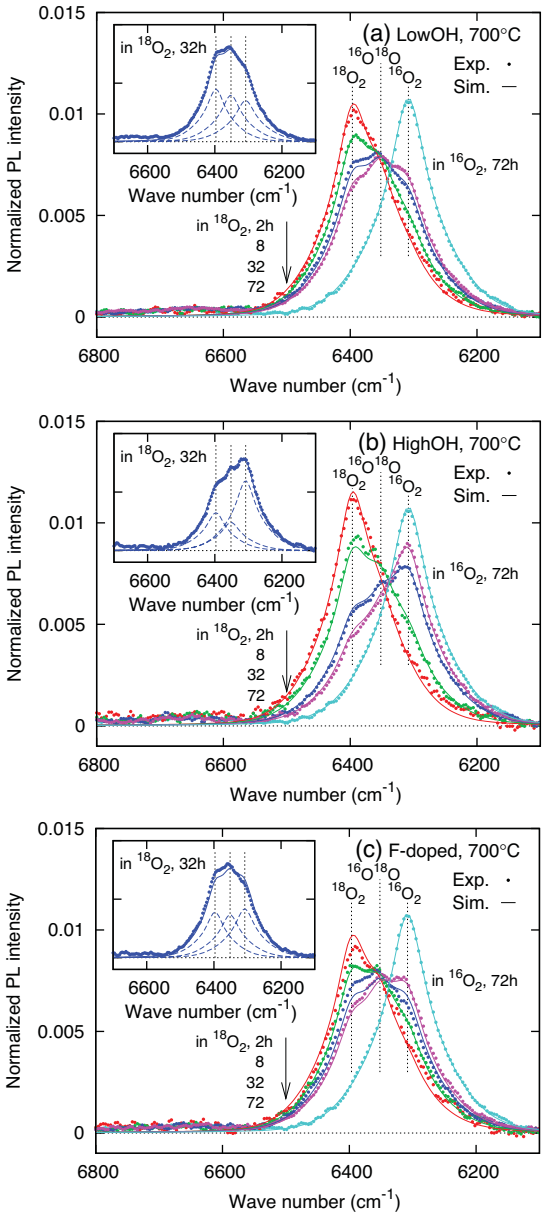

FIG. 3. (Color online) VSB spectra of the (a) LowOH, (b) HighOH, and (c) F-doped samples treated at 700 °C in $^{16}O_2$ or $^{18}O_2$. The ordinate scale is identical to the spectrum shown in Fig. 1. Dotted curves indicate experimental spectra. Simulated spectra denoted by solid lines are calculated from the solutions of rate equations[29] obtained by least-squares fits to the experimental spectra. The insets show VSB spectra of samples treated for 32 h and peak decompositions of the simulated spectra.

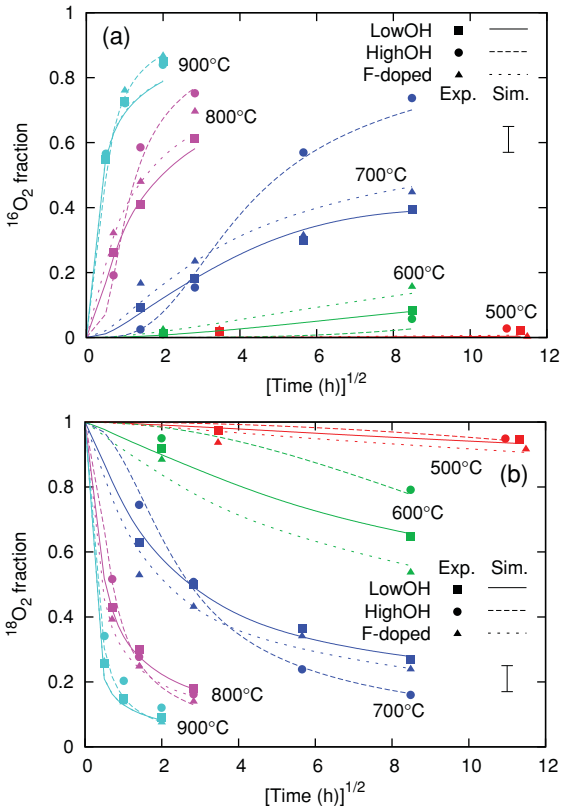

FIG. 4. (Color online) Variation of the fractions of interstitial (a) $^{16}O_2$, f_{66} and (b) $^{18}O_2$, f_{88}, with time and temperature of thermal annealing in $^{18}O_2$. Filled symbols are derived by simple VSB peak decomposition. Lines denote simulated curves calculated by simultaneously fitting all VSB spectra of the same type of sample. The error bar represents the experimental uncertainty.

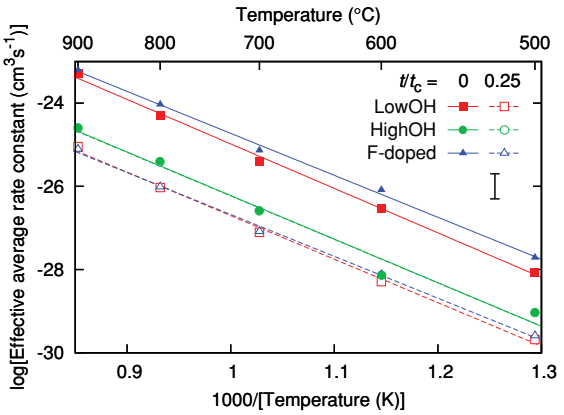

FIG. 5. (Color online) Arrhenius plots of effective average rate constant $k_{\mathrm{eff,a}}(t)$ [Eq. (20)] of oxygen exchange in the LowOH, HighOH, and F-doped samples calculated at $t/t_c = 0$ and 0.25. t_c is defined by $t_c = \pi(L/4)^2/D$, where L is sample thickness and D is the diffusion coefficient of interstitial O_2. $k_{\mathrm{eff,a}}$ represents the rate of transfer of ^{18}O from interstitial O_2 to a-SiO_2 at each moment, and is equal to k_a, the weighted average of k_i defined in Eq. (16) at $t = 0$. At $t/t_c = 0.25$, the average concentration of interstitial O_2 becomes one-half of the saturation concentration, i.e., $C_a^T(t/t_c = 0.25) = C_0^T/2$. For the HighOH sample, the data points at $t/t_c = 0$ and 0.25 are almost coincident. The error bars represent the experimental uncertainties.

Figure 6 also shows Arrhenius plots of $k_{\mathrm{eff,a}}$, drawn with k_{peak} and w defined in Eq. (4). In the HighOH sample, $k_{\mathrm{eff,a}}$ was relatively close to k_{peak}. In the LowOH and F-doped samples, however, $k_{\mathrm{eff,a}}$ was much larger than k_{peak} and did not overlap with the FWHM area. Thus, Figs. 5 and 6 clearly show that in the LowOH and F-doped samples, the network oxygen atoms belonging to the tail part of the distribution dominate oxygen exchange with interstitial O_2. In the HighOH sample, in contrast, a much larger number of network oxygen atoms participates in the oxygen exchange.

For an interstitial O_2 molecule, the average time interval of the oxygen exchange is given by $\Delta t_{\mathrm{ex}} = (k_a N^T)^{-1}$. Its substitution into the average diffusion length in one dimension, $l = 2(D\Delta t_{\mathrm{ex}}/\pi)^{1/2}$, yields the average exchange-free diffusion length of interstitial O_2 as

$$l = 2\left(\frac{D\Delta t_{\mathrm{ex}}}{\pi}\right)^{1/2} = 2\left(\frac{D}{\pi k_a N^T}\right)^{1/2}. \qquad (22)$$

Figure 7 summarizes l calculated for the LowOH, HighOH, and F-doped samples. l was ~10–100 μm at 500°C, but decreased with an increase in temperature. At 900 °C, l was an order of magnitude smaller than that at 500 °C. l of the HighOH sample was a bit larger than that of the LowOH and F-doped samples because of the smaller $k_a = k_{\mathrm{eff,a}}(t/t_c = 0)$, as shown in Fig. 5.

D. Numerical simulation of the distribution of ^{18}O in interstitial O_2 and the a-SiO_2 network

Figures 8(a)–8(c) show simulated cross-sectional profiles of C^T, C, C^*, and C^{**} that best reproduce the observed VSB spectra of the LowOH sample treated at 500, 700, and 900 °C (Fig. 3). At 500 °C, $^{18}O_2$ was the main form ($f_{88} \sim 0.93$, $f_{66} < 0.01$). Since the saturated O_2 concentration C_0^T was

TABLE III. Preexponential factor k_0 and activation energy ΔE_a for the average exchange rate constant k_a [Eq. (16)], effective average exchange rate constant $k_{\mathrm{eff,a}}$ [Eq. (20)] at $t/t_c = 0.25$, and exchange rate constant at the peak of the distribution k_{peak} [Eq. (4)], derived from data shown in Figs. 5 and 6. For k_{peak}, FWHM of the distribution of ΔE_a [note that this is not equal to w defined in Eq. (4)][28] is also shown.

	$k_a = k_{\mathrm{eff,a}}(t/t_c = 0)$		$k_{\mathrm{eff,a}}(t/t_c = 0.25)$		k_{peak}		
Type	k_0(cm^{3}s^{-1})	ΔE_a(eV)	k_0(cm^{3}s^{-1})	ΔE_a(eV)	k_0(cm^{3}s^{-1})	ΔE_a(eV)	FWHM(eV)
LowOH	5.1×10^{-15}	2.1	5.7×10^{-17}	2.1	2.9×10^{-8}	5.5	1.5
HighOH	1.8×10^{-16}	2.1	1.7×10^{-16}	2.1	3.0×10^{-15}	2.5	0.5
F-doped	2.3×10^{-15}	2.0	2.5×10^{-17}	2.0	1.4×10^{-8}	5.5	1.5

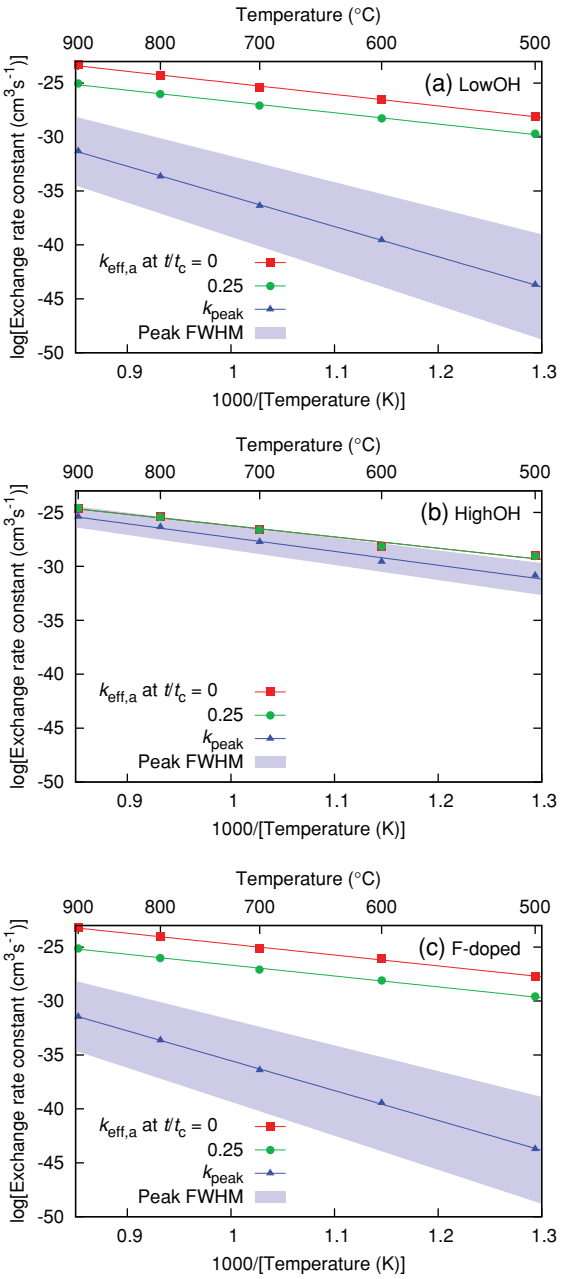

FIG. 6. (Color online) Arrhenius plots of exchange rate constants k for the (a) LowOH, (b) HighOH, and (c) F-doped samples. Both the rate constant at the peak of the distribution k_{peak} [Eq. (4)] and $k_{eff,a}$ calculated at $t/t_c = 0$ and 0.25 (same as Fig. 5) are shown. The shaded area denotes FWHM of the distribution w.

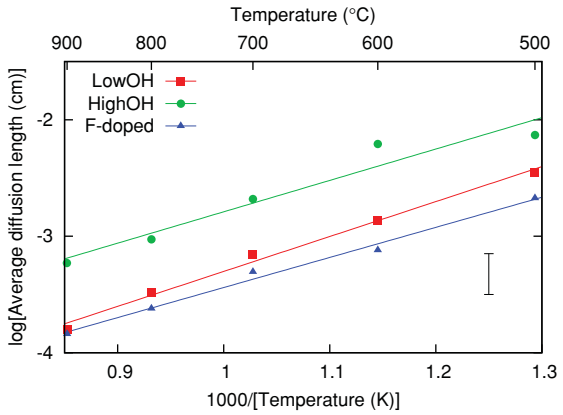

FIG. 7. (Color online) Temperature dependence of average exchange-free diffusion length l [Eq. (22)] of the LowOH, HighOH, and F-doped samples. The error bars represent the experimental uncertainties.

~5 orders-of-magnitude smaller than the concentration of the network oxygen atoms N^T, this result demonstrates that the oxygen exchange is very slow at 500 °C. However, it intensified with an increase in temperature, enhancing the formation of $^{16}O^{18}O$ and $^{16}O_2$. In the sample treated for 32 h at 700 °C, $^{16}O_2$ was dominant near the sample center, and $^{16}O^{18}O$ was the major form in the midway between the surface and sample center. At 900 °C, the oxygen exchange was much faster, resulting in a shallower penetration of $^{18}O_2$ and $^{16}O^{18}O$ and in a significantly broadened central $^{16}O_2$-rich region.

Figure 8(d) shows simulated cross-sectional profiles of N^*. The concentration profiles of ^{18}O atoms in interstitial O_2 ($C^* + 2C^{**}$) are also shown. The N^* and $C^* + 2C^{**}$ curves were nearly parallel in all data, indicating that N^* is simply proportional to the concentration of ^{18}O in interstitial O_2. $C^* + 2C^{**}$ at the surfaces was insensitive to temperature, whereas the ratio $N^*/(C^* + 2C^{**})$ increased with an increase in temperature due to the acceleration of the oxygen exchange. At 900 °C, however, near the sample center, N^* was significantly depressed despite the fast oxygen exchange, indicating that a rapid ^{18}O transfer from interstitial O_2 to the a-SiO_2 network near the surface hinders deeper penetration of ^{18}O. This is also a consequence of large ΔE_a for k_a as compared with ΔE_a for D; otherwise, profiles calculated at different temperatures would not cross.

Figure 9 compares simulated cross-sectional concentration profiles of network (N^*) and interstitial ($C^* + 2C^{**}$) ^{18}O atoms among the three types of samples annealed for 72 h at 700 °C. Partial contributions N_i^* due to the ith component in the exchange rate distribution [Eqs. (4) and (5)] are also plotted at $-5 \leqq i \leqq 15$. In all the plots, N^* was proportional to $C^* + 2C^{**}$, which is consistent with the results shown in Fig. 8(d). In the HighOH sample, all N_i^* profiles were nearly parallel with each other and $\log N_i^*$ changed linearly with x. Thus, $k_{eff}(x,t)$ varied little with x. N_i^* was the largest at $i \simeq$ 0–5, indicating that the network oxygen atoms belonging to the middle of the k distribution control the oxygen exchange. In the LowOH and F-doped samples, N_i^* was the largest at $i \gtrsim 10$, and thus the tail part of the distribution is the most important for the oxygen exchange. Here the component that gave the largest N_i^* value varied with x, and k_{eff} decreased with $|x|$. In addition, the $\log N_i^*(x)$ curves became flat at $i \gtrsim 10$, particularly near the surfaces, showing a sign of the saturation of the network oxygen atoms with ^{18}O ($N_i^* \simeq N_i^T$) because of large k_i and small N_i^T in these components. Consequently, the $\log N^*(x)$ profile became convex upward at the $x \neq 0$ region.

Figure 10 shows time dependence of thickness averages of N^* and N_i^* [N_a^* and $N_{a,i}^*$, respectively, derived by Eq. (18)] in the three types of samples treated at 700 °C. There is again a difference between the HighOH sample and the other two types of samples. In the LowOH and F-doped samples, the N_a^* profile

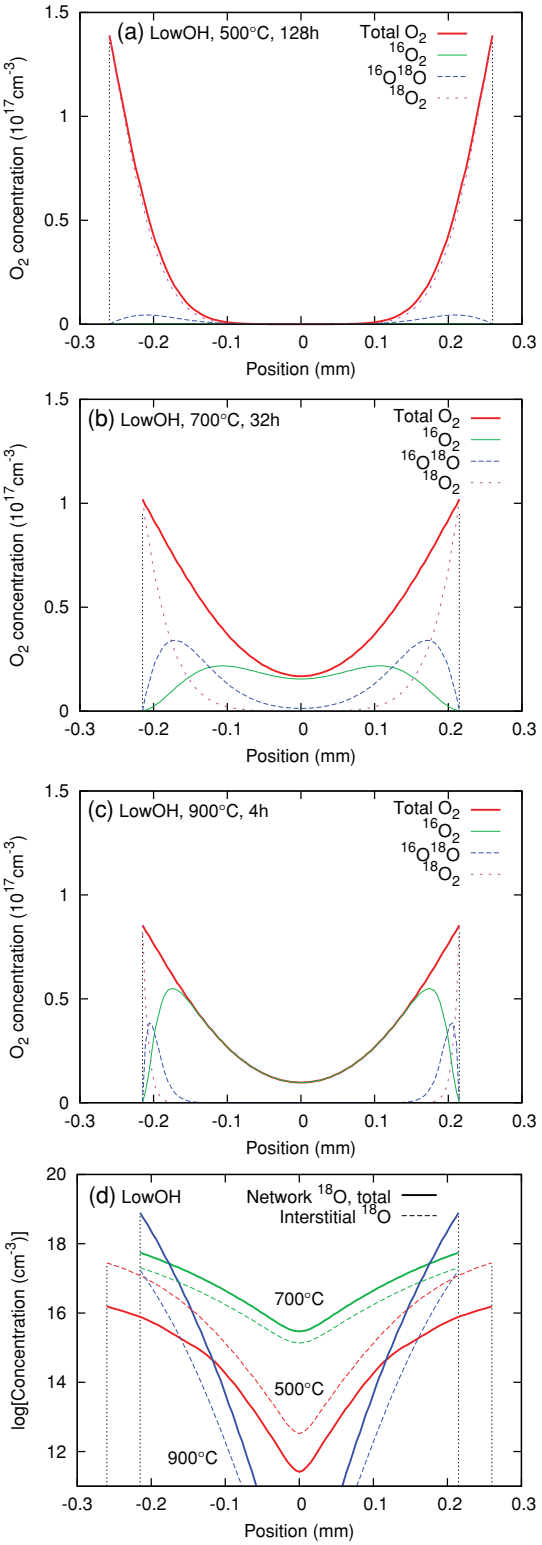

FIG. 8. (Color online) The effect of temperature on simulated cross-sectional concentration profiles of interstitial $^{16}O_2$, $^{16}O^{18}O$, and $^{18}O_2$ (C, C^*, and C^{**}, respectively) as well as their sum ($C^T = C + C^* + C^{**}$) in the LowOH samples. The data are taken from samples treated for (a) 128 h at 500 °C, (b) 72 h at 700 °C, and (c) 4 h at 900 °C . In panel (a), C is very small and the profile almost overlaps with the abscissa. The cross-sectional concentration profiles of ^{18}O atoms in the a-SiO_2 network and interstitial O_2 (N^* and $C^* + 2C^{**}$, respectively) in these samples are shown in panel (d).

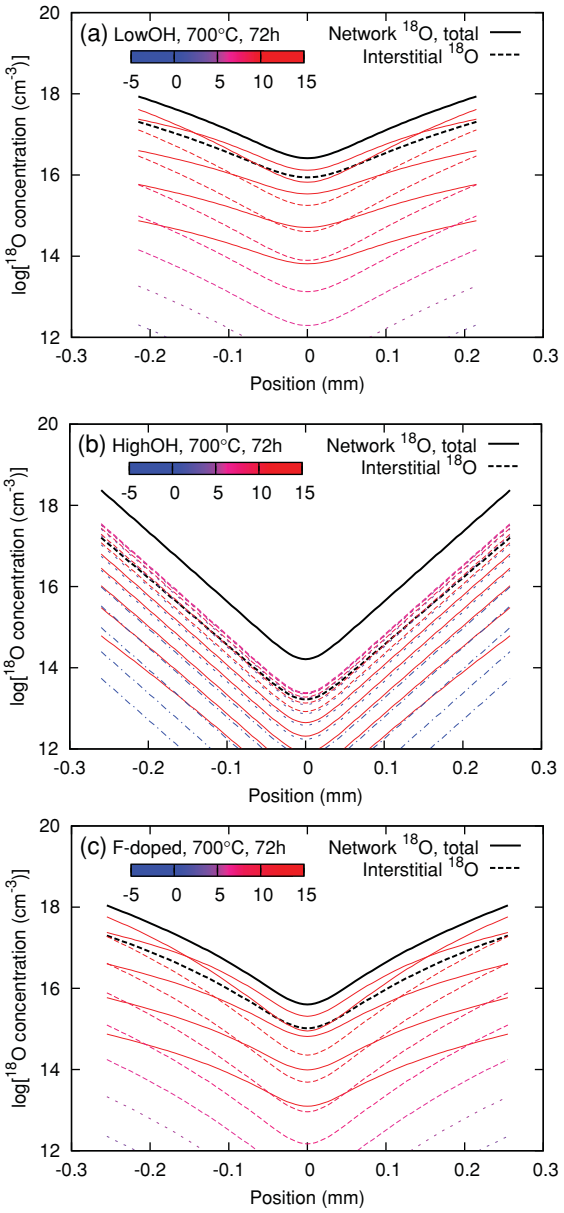

FIG. 9. (Color online) Simulated cross-sectional concentration profiles of the network ^{18}O atoms (N^*) in the (a) LowOH, (b) HighOH, and (c) F-doped samples treated for 72 h at 700 °C. The decomposition of the profiles into components N_i^*, which is associated with the exchange rate constant k_i [Eq. (5)], is also displayed for the i range $15 \geqq i \geqq -5$ (also see color bars): $15 \geqq i \geqq 11$, thin solid lines; $10 \geqq i \geqq 6$, thin dashed lines; $5 \geqq i \geqq 0$, thin dotted lines; and $-1 \geqq i \geqq -5$, thin dash-dotted lines. Thick dashed lines denote the concentration of ^{18}O atoms in interstitial O_2, $C^* + 2C^{**}$.

at small t ($\lesssim$4 h) was mainly determined by $N_{a,i}^*$ of components at $i \gtrsim 10$, because their k_i values were far larger than k_{peak} [Figs. 6(a)and 6(c)]. However, all N_i^T of such components were relatively small, resulting in an easy saturation of $N_{a,i}^*$ with t. Thus, i of the largest $N_{a,i}^*$ component decreased with an increase in t. In the HighOH sample, where the k_i distribution was narrow [Fig. 6(b)], all $N_{a,i}^*$ curves were almost parallel

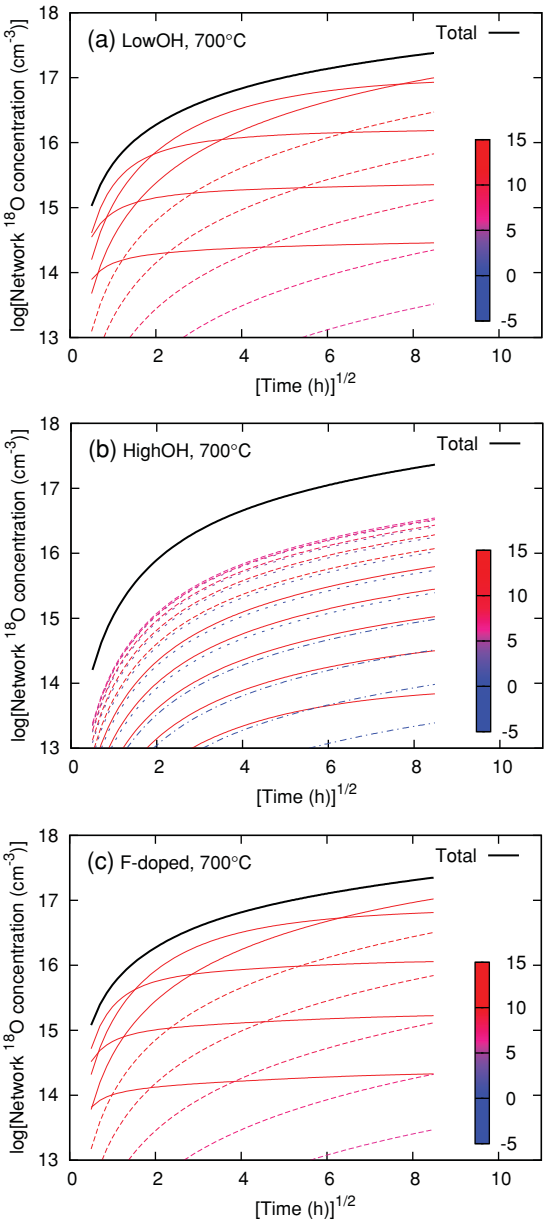

FIG. 10. (Color online) Simulated time-dependent change of thickness average of the concentrations of network ^{18}O atoms (N_a^*) in the (a) LowOH, (b) HighOH, and (c) F-doped samples treated at 700 °C. The components $N_{a,i}^*$ associated with the exchange rate constant k_i are also displayed for the i range $15 \geqq i \geqq -5$ (also see color bars): $15 \geqq i \geqq 11$, thin solid lines; $10 \geqq i \geqq 6$, thin dashed lines; $5 \geqq i \geqq 0$, thin dotted lines; and $-1 \geqq i \geqq -5$, thin dash-dotted lines.

with each other, and components with $i \simeq 0$–5 with N_i^T that are far larger than C_0^T dominate the oxygen exchange.

IV. DISCUSSION

In this study, we evaluated the second-order rate constant k defined on the basis of the oxygen exchange mechanism described by Eqs. (2) and (3). A remarkable finding is that activation energy ΔE_a for the average oxygen exchange rates k_a [Eq. (16)] and $k_{eff,a}$ [Eq. (20)] listed in Table III is insensitive to the presence of the network modifiers such as SiOH, SiF, and SiCl groups. Furthermore, k_a is influenced only a little by $\sim 10^{19}$ cm^{-3} SiF groups, and is even decreased by $\sim 10^{20}$ cm^{-3} SiOH groups (Fig. 5), indicating that the network modifiers do not serve as preferential oxygen exchange sites.

ΔE_a for k_a is ~2 eV. SIMS depth-profiling studies of the network ^{18}O atoms in a-SiO_2 samples treated in $^{18}O_2$ have reported similar ΔE_a values [~2.6 eV (Ref. 34) and ~1.7 eV (Ref. 13)], although these studies assumed first-order exchange processes. ΔE_a for k_a is larger than ΔE_a for diffusion of interstitial O_2 in a-SiO_2 (~0.8–1.2 eV) (see Refs. 2, 30, 22, 31, and 33; see also Table II). It is even larger than that for the permeation of interstitial N_2 (~1.4 eV) (Ref. 35) in which the N–N bond is unlikely to dissociate during the permeation. These results provide strong evidence that the oxygen exchange and the permeation of interstitial O_2 are independent processes. They are also consistent with the model that attributes the barrier for the O_2 permeation to the energy necessary to dilate openings connecting neighboring interstitial voids without breaking the a-SiO_2 network.[5,36–38]

On the other hand, ΔE_a for k_a is evidently smaller than the energy of the O–O bond in the O_2 molecule (~5.1 eV) and of an Si–O bond (~4.7 eV), which is close to the energy of the viscous flow of a-SiO_2 (~5–7 eV). (Refs. 39–41) Thus, ΔE_a for k_a most likely corresponds to the energy of the formation of activation complex during the oxygen exchange. ΔE_a of k_{peak} for the LowOH and F-doped samples is ~5–6 eV (Table III). It may relate to the energy of Si–O and O–O bonds described above. However, this agreement can also be accidental, because the value is influenced by the shape of the ΔE_a distribution, which may actually not be Gaussian.

Another important result is that the VSB spectra of the LowOH and F-doped samples are simulated well only when the distribution in k is introduced. We suggest that this k distribution is due to the site-to-site variation in ΔE_a for the oxygen exchange that originates from the structural disorder of a-SiO_2. A theoretical study[42] has reported similar site-to-site variation for the formation energy of the peroxy linkage (Si–O–O–Si; POL),[42–46] which may be transiently created along with the oxygen exchange. Interestingly, the calculated formation energy of POL is not a simple function of the Si–O–Si angle; it is instead strongly dependent on the deformation of a more extended a-SiO_2 network region.[42] In this context, it is unexpected that incorporation of $\sim 10^{19}$ cm^{-3} SiF groups does not significantly change k_a and w, although it is well known to enhance the structural relaxation by breaking up Si–O bonds and decomposing strained Si–O–Si bonds, typically occurring as small rings of 3 or 4 Si–O bonds, $(Si–O)_n$ ($n = 3, 4$).[47–49] Thus, the influence of the local network strain on oxygen exchange and the structure of preferential oxygen exchange sites are currently uncertain.

An important implication of the k distribution in the LowOH and F-doped samples shown in Figs. 6, 8, and 9 is that only a small part of the network oxygen atoms participates in the oxygen exchange. This may be simply because these network oxygen atoms are more reactive than the other network oxygen atoms. However, the present experiment does not exclude the possibility that only a limited number of network oxygen atoms is accessible to interstitial O_2, in other words, preferred "channels" for migration of interstitial O_2 may exist.[50] Recent theoretical calculations have also

suggested that the long-range diffusion of interstitial O_2 mainly involves the lowest-energy part of the energy landscape.[5,51] Nevertheless, experimental evidence is still insufficient to discuss the detail here.

The FWHM of k distribution w for the HighOH sample is much smaller than that of the LowOH and F-doped samples (Fig. 6 and Table III). It is unlikely that the decrease in w is a result of the breaking up of the a-SiO_2 network by SiOH groups and the consequent reduction of the local network strain,[52–54] because a similar decrease in w is not seen in the F-doped sample. The most probable origin of the small w is chemical reactions involving SiOH groups. For example, two SiOH groups are converted to an interstitial H_2O molecule and a network oxygen atom.[15,55–62] Since the resultant interstitial H_2O is mobile, this reversible reaction modifies the network topology by displacing SiOH groups, and spatially redistributes the network ^{18}O atoms as[15,56,57,59,63]

$$H_2^{18}O + \equiv Si-{}^{16}O-Si\equiv \rightleftarrows \equiv Si^{16}OH + H^{18}OSi\equiv \rightleftarrows H_2^{16}O + \equiv Si-{}^{18}O-Si\equiv. \quad (23)$$

The reaction given by Eq. (23) becomes fast enough to reach local equilibrium above ~600–700 °C.[17,60] Furthermore, analysis of diffusion of $H_2^{18}O$ in a-$Si^{16}O_2$ (Ref. 57) has confirmed that a large part of the network oxygen atoms participate in the reaction given by Eq. (23). Such a ^{18}O redistribution mechanism would be much faster in the HighOH sample than in the LowOH and F-doped samples, because the concentration of paired SiOH groups, which can be dehydrated easily, is roughly proportional to the square of the SiOH concentration. The local network topology may be modified too by the bond switching accompanied by hydrogen transfer between two network oxygen atoms; such reactions include the rotation of an SiO_4 tetrahedron,

$$\equiv O_3SiO^{\dagger}H \rightleftarrows \equiv O_2O^{\dagger}SiOH, \quad (24)$$

and the self-diffusion of an SiOH group,

$$\equiv Si^{\dagger}-O^{\dagger}H + \equiv Si-O-Si\equiv \rightleftarrows \equiv Si^{\dagger}-O^{\dagger}-Si\equiv + \equiv Si-OH. \quad (25)$$

Besides, a small amount of SiCl groups (~1/20 of SiOH concentration) embedded in the HighOH sample may add some difference in comparison to the LowOH and F-doped samples, because SiCl groups react with interstitial O_2 and H_2O molecules,[64]

$$2\equiv SiCl + 1/2O_2 \rightleftarrows \equiv Si-O-Si\equiv + Cl_2, \quad (26)$$

$$\equiv SiCl + H_2O \rightleftarrows \equiv SiOH + HCl. \quad (27)$$

The redistribution of network ^{18}O atoms and modification of the network topology by the reactions given by Eqs. (23)–(27) dynamically average the local environments of the ^{18}O-labeled network oxygen atoms, and this mechanism can explain the small w in the HighOH sample.

As shown in Fig. 8, the saturated O_2 concentration (C_0^T ~10^{17} cm^{-3}) is ~5 orders-of-magnitude smaller than the network oxygen concentration ($N^T = 4.41 \times 10^{22}$ cm^{-3}). This is the main reason for the small concentration of the network ^{18}O atoms (N^*, $\lesssim 10^{19}$ cm^{-3}) as compared with N^T, even after thermal annealing for 4 h at 900 °C [Fig. 8(d)]. In contrast, SIMS and NRA depth-profiling experiments have shown that $^{18}O_2$ treatment at ~900 °C commonly forms a ~1–10-nm-thick ^{18}O-rich layer, in which N^* is ~10^{21-22} cm^{-3}, near the outer surface of a-SiO_2.[8,13,34,65] This surface ^{18}O-rich layer is unrelated to the oxygen exchange evaluated in this study, because it is formed by more rapid ^{18}O flow from ambient $^{18}O_2$ gas to the a-SiO_2 network, which was not considered in this simulation. In fact, the formation of the surface ^{18}O-rich layer has been attributed to the redistribution of the network ^{18}O atoms by trace amounts of water [Eq. (23)],[6,17] because the self-diffusion of the network oxygen atoms is too slow to contribute to the profile.[15,25] This mechanism of redistribution of network ^{18}O atoms by traces of water is expected to be similar to the above-described processes observed in the HighOH sample in this study.

Beneath the surface ^{18}O-rich layer, a tail part, where N^* decreases much more gradually with the depth, is observed.[11,13] This tail part is believed to be formed by the oxygen exchange between interstitial O_2 and the a-SiO_2 network, and has been used to evaluate the oxygen exchange rate.[13,34] The reported N^* in the tail part is ~10^{19-20} cm^{-3} at 900–1000 °C,[11,13] showing a relatively good agreement with the value calculated in this study (~10^{19} cm^{-3} at 900 °C). The small discrepancy between these two values may be due to the very small depth of the observed tail profiles (~0.1–1 μm) compared with the thickness of samples used in this study (~0.4–0.5 mm). Thus, ^{18}O observed in the tail part may not solely be due to the oxygen exchange; traces of water incorporated from ambient atmosphere may still contribute to form the tail profile.

V. CONCLUSIONS

The $a^1\Delta_g(v=0) \rightarrow X^3\Sigma_g^-(v=1)$ infrared photoluminescence band of oxygen molecules (O_2) introduced in the interstitial voids in amorphous SiO_2 (a-SiO_2) undergoes an isotope shift as a result of ^{16}O–^{18}O substitution. This isotope shift was utilized to study quantitatively the oxygen exchange between the a-SiO_2 network and ^{18}O-labeled interstitial O_2 in synthetic a-SiO_2 with different concentrations of common network modifiers (SiOH, SiF, and SiCl groups). Incorporation of these network modifiers left almost unchanged or even decreased the average oxygen exchange rate, suggesting that they do not significantly participate in the oxygen exchange. The activation energy for the average oxygen exchange rate is ~2 eV, irrespective of the type and concentration of the network modifiers, and it is larger than that for the permeation of interstitial O_2 (~0.8–1.2 eV). Furthermore, the average exchange-free diffusion length of an interstitial O_2 molecule is ~1–100 μm in the temperature range between 500 and 900 °C, indicating that the oxygen exchange is not the bottleneck of the permeation of interstitial O_2 in a-SiO_2. The oxygen exchange rate is distributed because of the site-to-site variation of the reactivity of network oxygen atoms with interstitial O_2. However, the distribution of the oxygen exchange rate is narrower in samples with high (~10^{20} cm^{-3}) SiOH concentrations. This smaller width is probably not caused by a real decrease in the dispersion of the oxygen exchange rates. Rather, it may be caused by the mobile interstitial water molecules, transiently

formed by dehydroxylation of SiOH groups. They may react with the a-SiO_2 network to redistribute ^{18}O over the a-SiO_2 network and may dynamically average the local configuration around the network oxygen atoms. These results may provide further evidence for reactions involving traces of interstitial water molecules in a-SiO_2.

*kkaji@tmu.ac.jp

[1] M. L. Green, E. P. Gusev, and E. L. Garfunkel, J. Appl. Phys. **90**, 2057 (2001).
[2] F. J. Norton, Nature (London) **191**, 701 (1961).
[3] B. E. Deal and A. S. Grove, J. Appl. Phys. **36**, 3770 (1965).
[4] M. A. Lamkin, F. L. Riley, and R. J. Fordham, J. Eur. Ceram. Soc. **10**, 347 (1992).
[5] A. Bongiorno and A. Pasquarello, Phys. Rev. Lett. **88**, 125901 (2002).
[6] R. H. Doremus, J. Non-Cryst. Solids **349**, 242 (2004).
[7] W. Orellana, A. J. R. da Silva, and A. Fazzio, Phys. Rev. Lett. **87**, 155901 (2001).
[8] S. S. Cristy and J. B. Condon, J. Electrochem. Soc. **128**, 2170 (1981).
[9] J. A. Costello and R. E. Tressler, J. Electrochem. Soc. **131**, 1944 (1984).
[10] C. J. Han and C. R. Helms, J. Appl. Phys. **59**, 1767 (1986).
[11] C. J. Han and C. R. Helms, J. Electrochem. Soc. **135**, 1824 (1988).
[12] J. D. Cawley, J. W. Halloran, and A. R. Cooper, Oxid. Met. **28**, 1 (1987).
[13] J. D. Kalen, R. S. Boyce, and J. D. Cawley, J. Am. Ceram. Soc. **74**, 203 (1991).
[14] R. Rosencher, A. Straboni, S. Rigo, and G. Amsel, Appl. Phys. Lett. **34**, 254 (1979).
[15] R. Pfeffer and M. Ohring, J. Appl. Phys. **52**, 777 (1981).
[16] J. J. Ganem, I. Trimaille, P. André, S. Rigo, F. C. Stedile, and I. J. R. Baumvol, J. Appl. Phys. **81**, 8109 (1997).
[17] R. H. Doremus, *Diffusion of Reactive Molecules in Solids and Melts* (Wiley, New York, 2002).
[18] K. Kajihara, T. Miura, H. Kamioka, A. Aiba, M. Uramoto, Y. Morimoto, M. Hirano, L. Skuja, and H. Hosono, J. Non-Cryst. Solids **354**, 224 (2008).
[19] L. Skuja, B. Güttler, D. Schiel, and A. R. Silin, Phys. Rev. B **58**, 14296 (1998).
[20] K. Kajihara, T. Miura, H. Kamioka, M. Hirano, L. Skuja, and H. Hosono, Phys. Rev. Lett. **102**, 175502 (2009).
[21] K. Kajihara, S. Matsuishi, K. Hayashi, M. Hirano, and H. Hosono, J. Phys. Chem. C **111**, 14855 (2007).
[22] K. Kajihara, H. Kamioka, M. Hirano, T. Miura, L. Skuja, and H. Hosono, J. Appl. Phys. **98**, 013529 (2005).
[23] K. Kajihara, T. Miura, H. Kamioka, M. Hirano, L. Skuja, and H. Hosono, Appl. Phys. Express **2**, 056502 (2009).
[24] K. Kajihara, H. Kamioka, M. Hirano, T. Miura, L. Skuja, and H. Hosono, J. Appl. Phys. **98**, 013528 (2005).
[25] J. C. Mikkelsen Jr., Appl. Phys. Lett. **45**, 1187 (1984).
[26] A. G. Revesz, B. J. Mrstik, and H. L. Hughes, J. Electrochem. Soc. **134**, 2911 (1987).
[27] R. H. Doremus, J. Electrochem. Soc. **143**, 1992 (1996).
[28] w was assumed to be related to FWHM of the dispersion of the activation energy in eV (w') as $w = w'e/(2.303k_BT)$.
[29] In the actual calculation, Eq. (10) was solved first to derive C^T. Then Eq. (13) was calculated and this determined $2C^{**} + C^*$, N_i^*, and $N_i \equiv N_i^T - N_i^*$. Finally, these results are substituted into Eq. (9), and C^{**}, $C^* \equiv (2C^{**} + C^*) - 2C^{**}$, and $C = C^T - C^* - C^{**}$ were derived.
[30] K. Kajihara, T. Miura, H. Kamioka, M. Hirano, L. Skuja, and H. Hosono, J. Ceram. Soc. Jpn. **112**, 559 (2004).
[31] C. C. Tournour and J. E. Shelby, Phys. Chem. Glasses **46**, 559 (2005).
[32] J. Crank, *The Mathematics of Diffusion*, 2nd ed. (Oxford University Press, Oxford, 1975).
[33] K. Kajihara, T. Miura, H. Kamioka, M. Hirano, L. Skuja, and H. Hosono, Mater. Sci. Eng. B **173**, 158 (2010).
[34] J. D. Cawley and R. S. Boyce, Philos. Mag. A **58**, 589 (1988).
[35] K. Kajihara, M. Hirano, Y. Takimoto, L. Skuja, and H. Hosono, Appl. Phys. Lett. **91**, 071904 (2007).
[36] O. L. Anderson and D. A. Stuart, J. Am. Ceram. Soc. **37**, 573 (1954).
[37] D. K. McElfresh and D. G. Howitt, J. Am. Ceram. Soc. **69**, C237 (1986).
[38] J. E. Shelby, *Handbook of Gas Diffusion in Solids and Melts* (ASM International, Materials Park, OH, 1996).
[39] G. Hetherington, K. H. Jack, and J. C. Kennedy, Phys. Chem. Glasses **5**, 130 (1964).
[40] R. H. Doremus, J. Appl. Phys. **92**, 7619 (2002).
[41] H. Kakiuchida, K. Saito, and A. J. Ikushima, J. Appl. Phys. **93**, 777 (2003).
[42] M. A. Szymanski, A. L. Shluger, and A. M. Stoneham, Phys. Rev. B **63**, 224207 (2001).
[43] G. Pacchioni and G. Ieranó, Phys. Rev. B **56**, 7304 (1997).
[44] D. R. Hamann, Phys. Rev. Lett. **81**, 3447 (1998).
[45] L. Skuja, K. Kajihara, T. Kinoshita, M. Hirano, and H. Hosono, Nucl. Instrum. Methods Phys. Res. B **191**, 127 (2002).
[46] K. Kajihara, L. Skuja, M. Hirano, and H. Hosono, Phys. Rev. Lett. **92**, 015504 (2004).
[47] H. Hosono and Y. Ikuta, Nucl. Instrum. Methods Phys. Res. A **166-167**, 691 (2000).
[48] K. Saito and A. J. Ikushima, J. Appl. Phys. **91**, 4886 (2002).
[49] L. Skuja, K. Kajihara, Y. Ikuta, M. Hirano, and H. Hosono, J. Non-Cryst. Solids **345-346**, 328 (2004).
[50] J. F. Shackelford, J. Non-Cryst. Solids **49**, 299 (1982).
[51] A. Bongiorno and A. Pasquarello, Phys. Rev. B **70**, 195312 (2004).
[52] A. J. Ikushima, T. Fujiwara, and K. Saito, J. Appl. Phys. **88**, 1201 (2000).
[53] L. Skuja, H. Hosono, M. Hirano, and K. Kajihara, Proc. SPIE **5122**, 1 (2003).
[54] K. Kajihara, J. Ceram. Soc. Jpn. **115**, 85 (2007).
[55] A. J. Moulson and J. P. Roberts, Trans. Faraday Soc. **57**, 1208 (1961).
[56] W. G. Spitzer and J. R. Ligenza, J. Phys. Chem. Solids **17**, 196 (1961).
[57] G. J. Roberts and J. P. Roberts, Phys. Chem. Glasses **7**, 82 (1966).
[58] J. E. Shelby, J. Vitko Jr., and R. E. Benner, J. Am. Ceram. Soc. **65**, C59 (1982).
[59] S. Rigo, F. Rochet, B. Agius, and A. Straboni, J. Electrochem. Soc. **129**, 867 (1982).

[60]H. Wakabayashi and M. Tomozawa, J. Am. Ceram. Soc. **72**, 1850 (1989).
[61]Y. Morimoto, T. Igarashi, H. Sugahara, and S. Nasu, J. Non-Cryst. Solids **139**, 35 (1992).
[62]K. M. Davis and M. Tomozawa, J. Non-Cryst. Solids **201**, 177 (1996).
[63]A. G. Revesz and H. A. Schaeffer, J. Electrochem. Soc. **129**, 357 (1982).
[64]K. Kajihara, M. Hirano, L. Skuja, and H. Hosono, J. Appl. Phys. **98**, 043515 (2005).
[65]F. Rochet, B. Agius, and S. Rigo, J. Electrochem. Soc. **131**, 914 (1984).